Regularized inversion of aerosol hygroscopic growth factor probability density function: Application to humidity-controlled fast integrated mobility spectrometer measurements

Jiaoshi Zhang[1], Yang Wang[1,3], Steven Spielman[2], Susanne Hering[2], and Jian Wang[1]

[1]Center for Aerosol Science and Engineering, Washington University in St. Louis, St. Louis, Missouri, USA
[2]Aerosol Dynamics Inc, Berkeley, California, USA
[3]Department of Civil, Architectural and Environmental Engineering, Missouri University of Science and Technology, Rolla, Missouri, USA

Correspondence to: Jian Wang (jian@wustl.edu)

Abstract. Aerosol hygroscopic growth plays an important role in atmospheric particle chemistry and the effects of aerosol on radiation and hence climate. The hygroscopic growth is often characterized by a growth factor probability density function (GF-PDF), where the growth factor is defined as the ratio of the particle size at a specified relative humidity to its dry size. Parametric, least-square methods are the most widely used algorithms for inverting the GF-PDF from measurements of humidified tandem differential mobility analyzers (HTDMA) and have been recently applied to the GF-PDF inversion from measurements of the humidity-controlled fast integrated mobility spectrometer (HFIMS). However, these least square methods suffer from noise amplification due to the lack of regularization in solving the ill-posed problem, resulting in significant fluctuations in the retrieved GF-PDF and even occasional failures of convergence. In this study, we introduce nonparametric, regularized methods to invert aerosol GF-PDF and apply them to HFIMS measurements. Based on the HFIMS kernel function, the forward convolution is transformed into a matrix-based form, which facilitates the application of the nonparametric inversion methods with regularizations, including Tikhonov regularization and Twomey's iterative regularization. Inversions of the GF-PDF using the nonparameteric methods with regularization are demonstrated using HFIMS measurements simulated from representative GF-PDFs of ambient aerosols. The characteristics of reconstructed GF-PDFs resulting from different inversion methods, including previously developed least-square methods, are quantitively compared. The result shows that Twomey's method generally outperforms other inversion methods. The capabilities of Twomey's method in reconstructing the pre-defined GF-PDFs and recovering the mode parameters are validated.

1 Introduction

The hygroscopic growth of aerosol particles influences heterogeneous reactions, light extinction, and visibility, whereby aerosol water is most relevant for the direct radiative forcing of Earth's climate (Tang and Munkelwitz, 1994; Pilinis et al., 1995; Swietlicki et al., 2008). The ability of aerosols to absorb water depends mainly on their compositions, hence the

hygroscopic properties reflect the variability of the key chemical components (Gysel et al., 2007; Zheng et al., 2020). Therefore, the variation of aerosol hygroscopic growth can be used to infer the potential chemical composition, especially for small aerosols that are beyond the size range of the aerosol mass spectrometer. Aerosol hygroscopic growth under atmospheric relative humidity (RH) is commonly measured by a humidified tandem differential mobility analyzer system

35   (HTDMA) (Liu et al., 1978; Rader and McMurry, 1986; Swietlicki et al., 2008). In an HTDMA system, monodisperse particles classified by the 1st DMA are exposed to an elevated RH in a humidity conditioner, and the size distribution of humidified particles is then measured by a 2nd DMA and a particle detector using scanning mobility technique. The particle hygroscopic growth is then derived from the size distribution of the humidified particles. Recently, a humidity-controlled fast integrated mobility spectrometer (HFIMS) was developed. The HFIMS replaces the 2nd DMA and particle detector

40   within the HTDMA system with a water-based fast integrated mobility spectrometer (WFIMS), which captures the size distribution of humidified particles instantly (Pinterich et al., 2017a). As a result, the HFIMS drastically accelerates aerosol hygroscopic growth measurements (Pinterich et al., 2017b; Wang et al., 2019; Zhang et al., 2021), making it feasible to characterize ambient aerosol hygroscopic growth at a wide range of sizes and RH levels under ~ 25 min.

The HTDMA measurement, i.e., the mobility-concentration distribution of humidified particles, is a convolution of the

45   aerosol hygroscopic growth factor probability density function (GF-PDF) and the transfer functions of both DMAs. Similarly, the HFIMS measurement represents a convolution of the aerosol GF-PDF together with the transfer functions of the DMA and the WFIMS (Wang et al., 2019). Two inversion algorithms, TDMAfit (Stolzenburg and McMurry (1988)) and TDMAinv (Gysel et al. (2009)) were developed and widely used to retrieve the GF-PDF from HTDMA measurements. In both algorithms, the GF-PDF is represented with a specific functional form, and the function parameters were derived by

50   least-squares fitting. For example, the TDMAfit algorithm assumes the GF-PDF as a superposition of multiple Gaussian distribution functions (Stolzenburg and McMurry, 1988) or a summation of multiple lognormal (ML) distribution functions (Stolzenburg and McMurry, 2008). Likewise, TDMAinv describes the GF-PDF as a piecewise linear (PL) function at predefined growth factor values (Gysel et al., 2009). The function parameters are derived using least-squares fitting that minimizes the residual between the measured and reconstructed size distributions of humidified particles. Similar methods

55   have been applied to invert GF-PDFs from HFIMS measurements by Wang et al. (2019).

Inversion of the GF-PDF from the HTDMA or HFIMS measurements is an ill-posed problem (Gysel et al., 2009). Least-squares methods such as TDMAfit and TDMAinv provide simple and effective ways to solve this ill-posed problem by representing the GF-PDF in a specific functional form (Kandlikar and Ramachandran, 1999). However, the GF-PDF inverted by the TDMAfit algorithm often relies on the initial guess of the parameters, resulting in occasional failures of convergence

60   (Gysel et al., 2009). For example, it was reported that the TDMAfit algorithm may not be robust in cases of closely multiple overlapped modes and the successful convergence depends on the initial guess (Swietlicki et al., 2008). Moreover, it is well-known that the unregularized least-squares method amplifies the measurement noise (Kandlikar and Ramachandran, 1999; Sipkens et al., 2020), resulting in significant fluctuations in the retrieved GF-PDF. It has been shown that the derived GF-PDF using the TDMAinv algorithm may oscillate strongly when a higher bin resolution is chosen, while a too low resolution

65   may not be adequate to reproduce complex shapes of true GF-PDF (Gysel et al., 2009). This may lead to incorrect interpretation of the aerosol mixing state (Wang et al., 2019). The approach to overcoming noise amplification is to regularize the problem by including additional information, such as smoothness (Kandlikar and Ramachandran, 1999). Tikhonov regularization is among the most common regularization methods and has been applied to inversions of the aerosol size distribution (Talukdar and Swihart, 2003) and mass-mobility distribution (Sipkens et al., 2020). Recently, a software

70   package was developed to invert HTMDA data using Tikhonov regularization (Petters, 2021). Twomey's algorithm (Twomey, 1975), one of the most common iterative regularization methods, has been widely used to invert aerosol size distributions (Collins et al., 2002; Olfert et al., 2008; Wang et al., 2018) and two-dimensional mass-mobility distributions (Rawat et al., 2016; Sipkens et al., 2020). However, to our best knowledge, the Twomey's algorithm has not been applied to invert GF-PDF from HTDMA or HFIMS measurements.

75   In this study, we present nonparametric, regularized inversions of the GF-PDF from HFIMS measurements. These inversion methods can be adapted to HTMDA measurements straightforwardly. The forward model (i.e., the convolution of the GF-PDF, the transfer function of DMA, and the transfer function of WFIMS) is derived analytically and cast into a matrix form such that nonparametric inversion methods can be conveniently applied. The nonparametric inversions are demonstrated by retrieving GF-PDF from HFIMS measurements of ambient aerosols. The dependence of retrieved GF-PDF on GF bin

80   resolutions is investigated, and an optimal GF bin resolution is identified. Synthetic data are generated using representative GF-PDFs of ambient aerosols and are applied to evaluate different inversion methods, including (1) parametric, least-squares fittings, (2) nonparametric, unregularized least-squares, (3) Twomey's algorithm, and (4) Tikhonov regularization. The performances of the different inversion methods including reconstruction accuracy, GF-PDF fidelity, smoothness, and computation time are presented and discussed.

2 Methods

85

This section presents the GF-PDF inversion routine from the HFIMS measurement, which includes the mathematical derivation of the matrix-based inverse problem, the description of different inversion algorithms, and the generation of synthetic data for evaluating the inversion algorithms.

2.1 A matrix form for the forward model

90   The integrated response of HFIMS is determined by the aerosol size distribution, the DMA transfer function, the GF-PDF, and the WFIMS transfer function Wang et al. (2019). The number concentration of particles with diameters between D_{p1} and $D_{p1} + \mathrm{d}D_{p1}$ downstream of the DMA inside the HFIMS is given by:

$$\mathrm{d}N_{\mathrm{DMA}} = \frac{Q_{\mathrm{a,DMA}}}{Q_{\mathrm{s,DMA}}} \eta_{\mathrm{chg}}(D_{\mathrm{p1}}) \eta_{\mathrm{p,DMA}}(D_{\mathrm{p1}}) \Omega(V_{\mathrm{DMA}}, \tilde{Z}_{\mathrm{p1}}) \mathrm{d}N \qquad (1)$$

where $Q_{a,DMA}$ and $Q_{s,DMA}$ are the DMA aerosol and sample (i.e., monodispersed) flow rates, respectively, $\eta_{chg}(D_{p1})$ is the aerosol charging efficiency, $\eta_{p,DMA}(D_{p1})$ is the particle penetration efficiency through the DMA, and $\Omega(V_{DMA}, \tilde{Z}_{p1})$ is the transfer function of the DMA operated with the classifying voltage of V_{DMA}, $\tilde{Z}_{p1}$ is the particle mobility (Z_{p1}) normalized by the DMA centroid mobility corresponding to V_{DMA}. $dN = n(D_{p1})dD_{p1}$ represents the number concentration of particles with diameters between D_{p1} and $D_{p1} + dD_{p1}$. The number concentration of particles with diameters between D_{p2} and $D_{p2} + dD_{p2}$ at the outlet of the conditioner is

$$dN_{cond} = dD_{p2} \int_{D_{p1}=0}^{D_{p1}=\infty} \eta_{p,cond}(D_{p2}) c_{cond}(D_{p2}, D_{p1}) dN_{DMA} \tag{2}$$

where the integration considers all possible values of D_{p1}. $\eta_{p,cond}(D_{p2})$ is the penetration efficiency of the conditioned particles, assuming the particle growth from D_{p1} to D_{p2} is instantaneous. $c_{cond}(D_{p2}, D_{p1})$ is the growth factor probability density function (GF-PDF) for particles with a dry diameter of D_{p1} growing to a diameter of D_{p2} during the humidity conditioning process. The GF-PDF satisfies $\int_{D_{p2}=0}^{D_{p2}=\infty} c_{cond}(D_{p2}, D_{p1}) dD_{p2} = 1$.

The WFIMS response to particles with diameters between D_{p2} and $D_{p2} + dD_{p2}$ in the ith D_p^* bin during any time interval (t) is calculated by

$$dR_i = \frac{Q_{a,WFIMS} N_F}{\dot{N}_F} \eta_{p,WFIMS}(D_{p2}) \eta_{det}(D_{p2}) \Omega_{WFIMS,i}(Z_{p2}) dN_{cond} \tag{3}$$

$Q_{a,WFIMS}$ is the inlet flow rate through the WFIMS, N_F is the number of frames being used to count dR_i, $\dot{N}_F$ is the frame rate. $N_F/\dot{N}_F$ represents the time interval (t) of counting, $\eta_{p,WFIMS}$ is the penetration efficiency of particles going through the WFIMS separator, $\Omega_{WFIMS,i}(Z_{p2})$ is the transfer function of the ith bin of the instrument response diameter (D_p^*) of the WFIMS. Note that the detection efficiency for particles above 8 nm has been shown to be 1 (i.e., $\eta_{det}(D_{p2}) = 1$, Pinterich et al., 2017a).

The theoretical response of the ith D_p^* bin of the HFIMS, R_i, can be derived by combining the above equations as detailed in Wang et al. (2019):

$$R_i = E \iint \frac{1}{D_{p1}} c_{cond}(g, D_{p1}) \Omega(V_{DMA}, \tilde{Z}_{p1}) \Omega_{WFIMS,i}(Z_{p2}) dD_{p2} dD_{p1} \tag{4}$$

Where $E = R_{tot} \frac{b}{b_{view}} \frac{Q_{sh,DMA}}{Q_{a,DMA}} \frac{d\tilde{Z}_{p1}}{dD_{p1}}\Big|_{D_{p1}^*}$. R_{tot} is the total counts of particles detected within the WFIMS viewing window, i.e., $R_{tot} = \sum_i R_i$, where R_i is the response of the ith D_p^* bin of the WFIMS. b_{view} and b are the length of the viewing area of the CCD-captured image and the length of the WFIMS mobility separator. In Eq. (4), the GF-PDF is written as a function of growth factor g (i.e., D_{p2}/D_{p1}), and it satisfies $c_{cond,n}(g, D_{p1})dg = c_{cond}(D_{p2}, D_{p1})dD_{p2}$. Given the narrow particle size range classified by the DMA, we assume the GF-PDF is the same for all particles classified by the DMA at a given voltage,

i.e., $c_{\text{cond}}(g, D_{p1})$ is independent of D_{p1} for the integration in Eq. (4). Rewriting the GF-PDF as $c_{\text{cond}}(g)$ and replacing D_{p2} with $g D_{p1}$ in Eq. (4) gives:

$$R_i = E \int_0^{+\infty} dg \, c_{\text{cond}}(g) \int_0^{+\infty} dD_{p1} \Omega\big[V_{\text{DMA}}, \tilde{Z}_{p1}(D_{p1})\big] \Omega_{\text{WFIMS},i}\big[Z_p(g D_{p1})\big] \quad (5)$$

125   The integration can be written as a sum over J GF bins, with the assumption that $c_{\text{cond}}(g)$ is a constant value within each GF bin:

$$R_{i,\text{theo}} = E \sum_{j=1}^{J} c_{\text{cond}}(g_j) \int_{g_{j-\frac{1}{2}}}^{g_{j+\frac{1}{2}}} dg \int_0^{+\infty} dD_{p1} \Omega\big[V_{\text{DMA}}, \tilde{Z}_p(D_{p1})\big] \Omega_{\text{WFIMS},i}\big[Z_p(g D_{p1})\big] \quad (6)$$

where $g_{j-1/2}$ and $g_{j+1/2}$ ($j = 1, 2, 3, …, J$) are the lower and upper bounds of the jth GF bin. Eq. (6) can be further arranged into a matrix form as

130 $$\mathbf{R} = \mathbf{M} \times \mathbf{c} \quad (7)$$

where the HFIMS response $\mathbf{R}$ is an $I \times 1$ array composed of R_i ($i = 1, 2, 3, …, I$). I is the selected size bins of the WFIMS that covers the size range of $(0.8 D_{p1}^*, 2.0 D_{p1}^*)$ according to the settings of the DMA centroid diameter D_{p1}^*. The unknown GF-PDF $\mathbf{c}$, an $J \times 1$ array composed of c_j ($j = 1, 2, 3, …, J$), can be found by solving the Fredholm integral equation (7). The element of the HFIMS kernel matrix, $\mathbf{M}$, is calculated by

135         $$M_{ij} = E_i \int_{g_{j-\frac{1}{2}}}^{g_{j+\frac{1}{2}}} dg \int_0^{+\infty} dD_{p1} \Omega\big[V_{\text{DMA}}, \tilde{Z}_p(D_{p1})\big] \Omega_{\text{WFIMS},i}\big[Z_p(g D_{p1})\big] \quad (8)$$

The HFIMS kernel describes the probability of particles with GF between $g_{j-1/2}$ and $g_{j+1/2}$ that is measured between the channel limits between $Z_{p,i-1/2}^*$ and $Z_{p,i-1/2}^*$. As described above, the inversion of the GF-PDF ($\mathbf{c}$) becomes an ill-posed problem due to overlapping of the HFIMS kernel function, like that of the aerosol size spectrometers (Kandlikar and Ramachandran, 1999; Collins et al., 2002; Talukdar and Swihart, 2003). It is worth noting that the derivation of the HFIMS

140   kernel function can be easily applied to HTDMA measurement by replacing the WFIMS transfer function $\Omega_{\text{WFIMS},i}\big[Z_p(g D_{p1})\big]$ with the transfer function of the 2nd DMA $\Omega\big[V_i, Z_p(g D_{p1})\big]$ in Eq. (8), where V_i is the classifying voltage of the 2nd DMA.

2.2 Inversion methods

A number of techniques have been developed to solve the Fredholm integration (Kandlikar and Ramachandran, 1999). With

145   Eqs. (7) and (8), nonparametric algorithms can be straightforwardly applied to invert GF-PDF, hence no prior knowledge of the functional form of GF-PDF is needed.

Unregularized least-squares

The simplest route is the ordinary least-squares (LSQ) which seeks to minimize the square of the residual:

$$\mathbf{c}^{LSQ} = arg \min_{\mathbf{c}} \{ \|\mathbf{Mc} - \mathbf{R}\|_2^2 \} \quad (9)$$

150   where $\|\cdot\|_2$ denotes the Euclidean norm. Here, the least-squares solution is solved by using the *lsqnonneg* function from
MATLAB.

Tikhonov regularization

Tikhonov regularization is a common regularization method that overcomes noise amplification, and it has been used to
invert aerosol size distribution and 2-D aerosol mass-mobility distributions (Talukdar and Swihart, 2003; Sipkens et al.,
155   2020). In Tikhonov regularization, an additional regularization term is included in the least-squares approach:

$$\mathbf{c}^{Tik} = arg\ \min_{\mathbf{c}}\{\|\mathbf{Mc} - \mathbf{R}\|_2^2 + \lambda^2\|\mathbf{Lc}\|_2^2\} \tag{10}$$

where $\lambda^2\|\mathbf{Lc}\|_2^2$ represents the regularization term designed to minimize the derivative of a specific order and λ is the
regularization parameter that controls the degree of regularization. The penalization matrix $\mathbf{L}$ is often set as the identity
matrix $\mathbf{I}$, the bidiagonal (-1, 1) matrix, and the upper tridiagonal (1, -2, 1) matrix for the 0th, 1st, and 2nd order regularization,
160   respectively (Hansen and O'Leary, 1993; Hansen, 1994). The parametric L-curve of $\|\mathbf{Mc}_\lambda - \mathbf{R}\|_2$ vs $\|\mathbf{Lc}_\lambda\|_2$ is plotted and
the corner of the L-curve is identified as the optimal regularization parameter λ which corresponds to a good balance
between minimization of the residual and reduction of the noise level (Hansen, 1992; Hansen and O'Leary, 1993).

Twomey's method

Twomey's method is commonly used to find solutions for ill-posed problems and has been proved to be effective in
165   inversions of the aerosol size distribution (Collins et al., 2002; Olfert et al., 2008) and aerosol mass-mobility distribution
(Rawat et al., 2016; Sipkens et al., 2020). It is a non-linear optimization method and provides iterative regularizations. An
initial guess solution is iteratively multiplied by small multiples of the HFIMS kernel function which are proportional to the
ratio of the measured to calculated measurements as follows:

$$c_j^{k+1} = \left[1 + \left(\frac{R_i}{\mathbf{m}_i\mathbf{c}^k} - 1\right)M_{ij}\right] \cdot c_j^k \tag{11}$$

170   where $\mathbf{m}_i$ is the ith row of the HFIMS kernel function $\mathbf{M}$, and $R_i/\mathbf{m}_i\mathbf{c}^k$ denotes the relative divergence between actual and
reconstructed HFIMS measurements. The positively constrained, least-squares solution is set as the initial guess (Olfert et
al., 2008). Then, the initial guess is smoothed using a three-term moving average (Markowski, 1987) and input into the
iterative Twomey's routine which is then repeated until a Chi-squared criterion is satisfied.

Parametric LSQ fittings

175   The parametric fitting methods assume a prior known distribution of the GF-PDF and calculate the forward model problem
(Eq. 4) to reconstruct the HFIMS measurements. A nonlinear least-squares fitting with boundary constraints is performed to
search for the least-squares solution within the bounds. The ML and PL fitting routines for the GF-PDF inversion from
HFIMS measurements have been developed by Wang et al. (2019). The influence of counting statistics and GF-PDF
parameters (i.e., the number of modes of ML GF-PDF and the number of sections of PL GF-PDF) has been statistically

180 studied. In this work, the GF-PDF inverted using ML and PL fitting routines with the optimized parameters are compared
with those retrieved using nonparametric inversion methods described above.

2.3 Generation of synthetic data to evaluate inversion algorithms

HFIMS measurements are synthesized to evaluate the performance of different inversion methods. The synthetic data are
based on three representative GF-PDF that consist of one, two, and three lognormal modes, respectively. The mode
185 parameters of the pre-defined GF-PDFs are listed in Table 1, similar to those listed in Wang et al. (2019). The parameters of
f, G, σ are the fractional weight, mean diameter growth factor, and geometric standard deviation of each mode. The
theoretical HFIMS response (i.e., R_i) is first derived using the Eq. (4) based on each of the three GF-PDFs. The actual FIMS
measurement follows the following Poisson distribution:

$$P(x) = \frac{R_i^x}{x!} \exp\left(-R_i\right) \tag{12}$$

190 where R_i is the derived theoretical response of the ith D_p^* bin, and $P(x)$ is the probability that x number of particles are
detected by HFIMS in the ith D_p^* bin (i.e., actual measurements). Five hundred sets of HFIMS measurements (R_i) are
generated using Monte Carlo methods based on the Poisson distribution for each D_p^* bin. Note that the total particle counts
detected during a typical HFIMS ambient measurement period (i.e., at least 20 seconds, Zhang et al., 2021) R_{tot} are set to
100 to maintain a constant counting statistic. These synthetic HFIMS measurements are used to evaluate the inversion
195 methods described above.

Table 1. Mode parameters of representative GF-PDFs for generating synthetic HFIMS measurements.

Predefined GF-PDF	Mode 1			Mode 2			Mode 3		
	f	G	σ	f	G	σ	f	G	σ
1	1.0	1.40	1.15		NA			NA	
2	0.45	1.10	1.05	0.55	1.30	1.05		NA	
3	0.39	1.05	1.10	0.32	1.40	1.05	0.29	1.70	1.10

3 Results and discussion

3.1 Optimal numbers of Growth factor bins and HFIMS size bins (D_p^*)

The numbers of GF bins (J) and D_p^* bins (I) determine the dimensions of HFIMS kernel function, which affects the
200 inversion of GF-PDF. The optimal number of D_p^* bin is a trade-off between sizing resolution and counting statistics. Wang
et al. (2019) examined the influence of WFIMS D_p^* bin number (I) on the inverted GF-PDF and found that an optimal range
of 23-32 for a total particle counts of 100. For representative remote continental and urban aerosols, the number of particles
measured by the HFIMS often exceed 100 in 20 seconds (Pinterich et al., 2017b; Zhang et al., 2021). The dynamic range of
WFIMS is roughly a factor of 10 in mobility, corresponding to a factor of ~3 in the size range (Zhang et al., 2021). In this

205 study, 30 size bins (i.e., $I = 30$) that are evenly spaced on a logarithmic scale over the WFIMS size range are used in the

inversions.

The influence of growth factor bin number (J) on the inverted GF-PDF is examined using the synthetic HFIMS measurements described above. The GF-PDF was inverted from each set of the simulated HFIMS measurements using different GF bin numbers ranging from 10 to 50 (i.e., corresponding to a GF resolution range of 0.024 - 0.12). To facilitate

210 the comparison of GF-PDFs inverted with different GF bin numbers, we interpolate the inverted GF-PDFs to 120 fixed growth factors that are evenly distributed from 0.8 to 2.0. The average error of the inverted GF-PDF γ is defined as:

$$\gamma^2 = \frac{1}{N}\sum_{i=1}^{N}\left(c_{i,inv} - c_{i,sim}\right)^2 \tag{13}$$

where $c_{i,inv}$ and $c_{i,sim}$ are the interpolated GF-PDF and pre-defined GF-PDF (i.e., true values) at the 120 fixed growth

factors, respectively. N is the number of points of fixed growth factors (i.e., 120). The smoothness of the inverted GF-PDF is

215 evaluated using the absolute second-order derivative:

$$\xi = \sum_{i=2}^{N-1}|2c_{inv}(g_i) - c_{inv}(g_{i+1}) - c_{inv}(g_{i-1})| \tag{14}$$

To evaluate how well the inverted GF-PDF reproduces the HFIMS measurement, we define the residual of the reconstructed FIMS measurement (i.e., reconstruction error) as:

$$\chi^2 = \sum_{i=1}^{L}\left(\tilde{R}_{i,inv} - \tilde{R}_i\right)^2 \tag{15}$$

220 where $\tilde{R}_{i,inv}$ is the normalized FIMS measurement that is reconstructed using Eq. (7) (i.e., forward calculation). $\tilde{R}_i$ is the normalized synthetic HFIMS measurement (i.e., true values).

Figure 1 shows the smoothness of the GF-PDF inverted using Twomey methods (ξ) versus the residual of reconstructed HFIMS measurement (χ^2) for different GF bin numbers (J). The variation of ξ with χ^2 exhibits an L-shaped curve for all three representative PF-PDF. The initial increase of J from 10 to 20 substantially improves the agreement between the

225 reconstructed and simulated HFIMS measurements, as indicated by a much reduced χ^2 value. At the same time, ξ remains relatively small, indicating a high smoothness of the inverted GF-PDF. In contrast, an increase of J above 20 leads to a minor reduction of χ^2 value but a drastic increase of ξ, suggesting strong noise in inverted GF-PDF. The optimal solution lies near the corner of the "L-curve" (Hansen and O'Leary, 1993) that strikes a balance between smoothness and fidelity to the HFIMS measurements. For all three pre-defined GF-PDFs, the corner of the L-curve corresponds to a J value of 20. GF-PDF

230 inverted with 20 growth factor bins generally shows the smallest error (γ^2), indicating best agreements between the inverted and the true GF-PDFs. The same type of L-curves for GF-PDFs inverted using unregularized LSQ and Tikhonov regularization are shown in the supplementary information (SI), and they also reveal a corner that corresponds to a J value of 20. These results suggest an optimal J value of 20 for a range of representative GF-PDFs and different inversion methods.
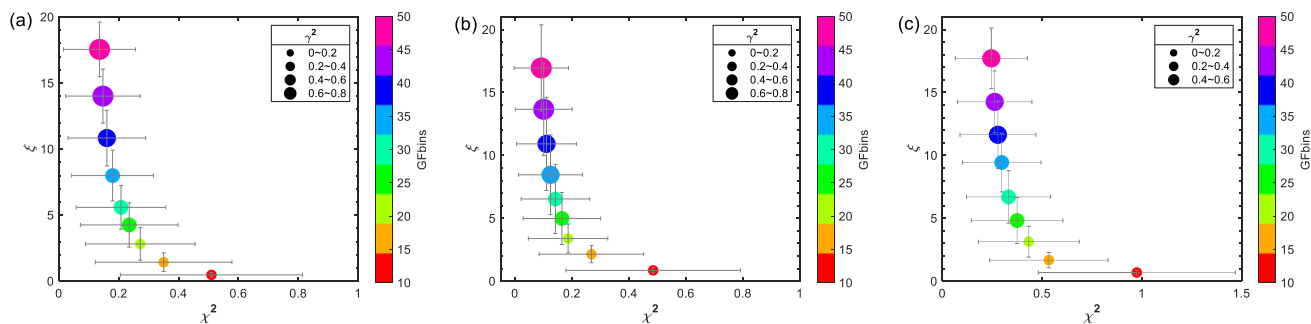
Figure 1. "L-curve" showing the dependence of reconstruction residual, χ^2, and the smoothness, ξ, on the number of GF bins of pre-defined GF-PDFs with (**a**) one mode, (**b**) two modes, and (**c**) three modes, respectively. The symbol size represents the error in inverted GF-PDF, γ^2. Whiskers represent standard deviation. The inversion is conducted using Twomey's method.

3.2 Comparisons of different inversion methods

In this section, we systematically compare the performance of different inversion methods described in Section 2.2. For all nonparametric methods, the inversions were carried out using the optimal numbers of GF bins (J) and D_p^* bins (I), 20 and 30, respectively. Figure 2 shows the residual of reconstructed HFIMS measurements (χ^2), the smoothness (ξ), the error of inverted GF-PDF residual (γ^2), and the computing time for different inversion methods. The results are the averages for the 500 sets of synthetic HFIMS data are shown for each of three pre-defined GF-PDFs. Compared with parametric counterparts (i.e., ML and PL least-squares fitting), the nonparametric methods generally retrieve more accurate GF-PDFs. Note that the ML least-squares fitting fails to converge to a valid solution occasionally, resulting in the abnormally large error in the inverted GF-PDFs, particularly for the pre-defined GF-PDFs with two and three modes. It may be due to the assumed spectral shape of GF-PDFs or the finite range of the boundary constraints that lead to a failure of searching for a least-squares solution in the presence of random noise. Among all nonparametric inversion methods, the unregularized LSQ provides the solution with the lowest reconstruction residual but largest noise and error in the inverted GF-PDFs, consistent with the noise amplification in unregularized methods. In comparison, regularized inversion methods generally produce smoother solutions at the expense of increased reconstruction residuals. Among different Tikhonov regularization methods, higher-order regularizations (i.e., 1st and 2nd) tend to produce smoother solutions, although the errors in inverted GF-PDF are very similar statistically. The ξ value of the GF-PDF inverted using 1st and 2nd order Tikhonov regularizations increase with the mode number of GF-PDF, consistent with the increasingly more complex spectral shape of GF-PDF. Overall, Twomey's method outperforms the other regularized inversion methods regardless of the shapes of the pre-defined GF-PDFs. On average, the GF-PDF inverted using Twomey's method has the smallest error (γ^2) and lowest ξ value, indicative of the outstanding de-noising performance.

Fig. 2(d) shows that once the matrix is generated, the implementation of the nonparametric methods requires a much shorter computing time than the parametric fitting methods. Here, the computing time is recorded on a desktop with Intel's 8th

260 generation processor Core i7-8700. On average, a single-time implement of any nonparametric method requires only ~1s for all three pre-defined GF-PDFs. In contrast, both ML and PL least-squares fitting routines require more than one order of magnitude longer time.
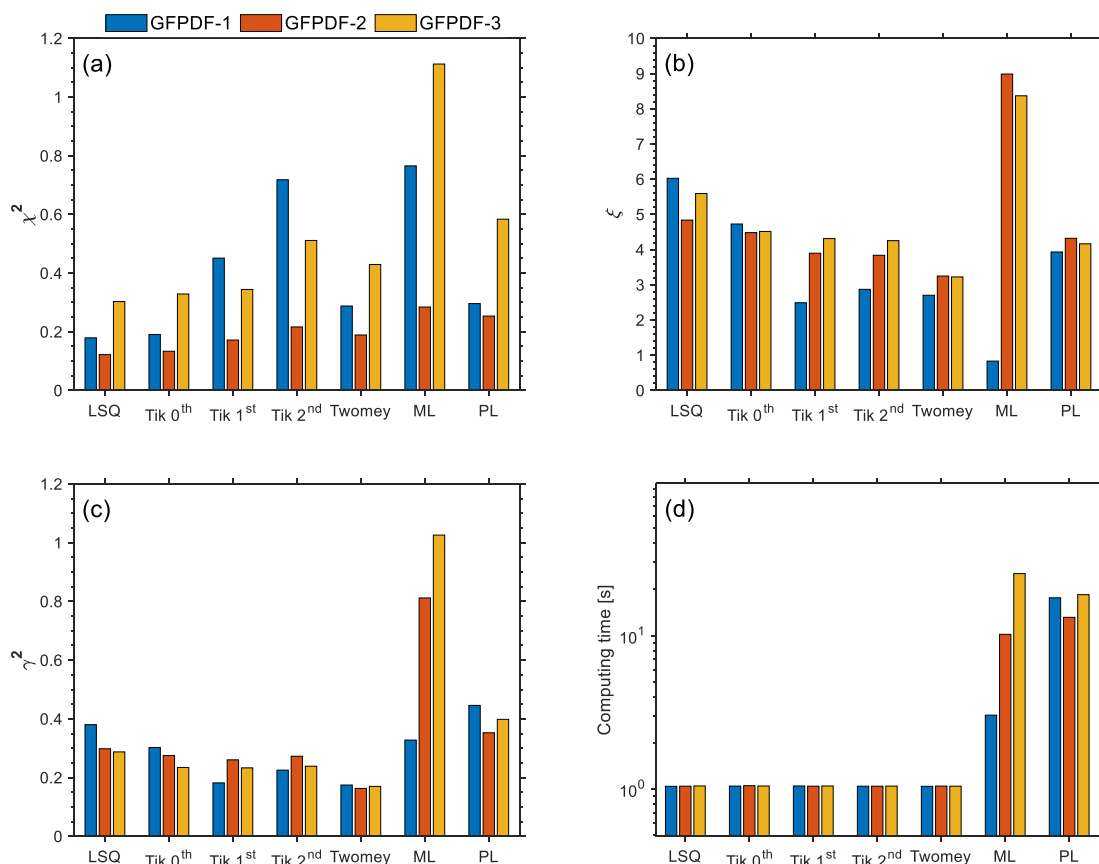
Figure 2. Comparison of reconstruction error, χ^2 (**a**), the degree of smoothing, ξ (**b**), the GFPDF residual, γ^2 (**c**) and the computing time (**d**) of inverted GF-PDFs using different inversion methods. Colors correspond to the pre-defined GF-PDFs with one mode (blue), two modes (orange), and three modes (yellow).

3.3 Inversion by Twomey's method

As Twomey's method is shown to be the best among all inversion methods examined, we examine the accuracy of inverted
270 GF-PDFs and the recovered mode parameters. Figure 3 compares the GF-PDFs inverted with the optimized GF and D_p^* bin numbers and with the pre-defined GF-PDFs. The reconstructed and the simulated HFIMS measurements are also presented in the top panel. Both the inverted GF-PDF and reconstructed HFIMS measurements are averaged over the inversions of 500 sets of synthetic data. The results demonstrate excellent agreement of the reconstructed HFIMS measurements with the synthetic data (i.e., simulated HFIMS measurements) for all three pre-defined GF-PDFs. Both the spectral shapes and peak
275 locations of the inverted GF-PDFs agreed well with that of the pre-defined GF-PDFs. In addition, the inverted GF-PDFs are

also in better agreement as compared with those inverted from parametric least-squares approaches (i.e., ML and PL GF-PDFs, Wang et al., 2019).
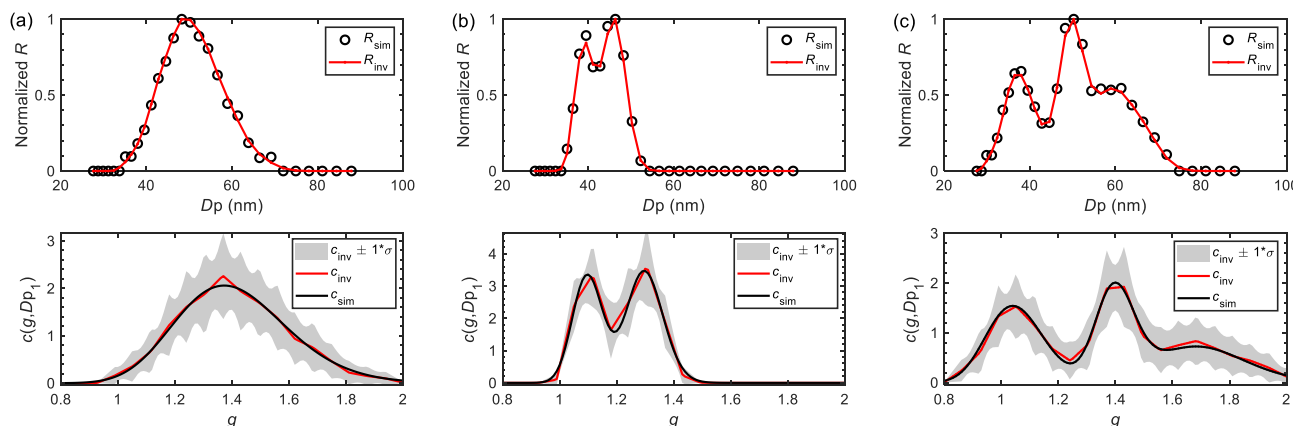
Figure 3. (*Top panels*) Comparisons between the averaged reconstructed HFIMS measurements and the simulated HFIMS measurements corrupted with Poisson noises for pre-defined GF-PDFs of one mode (**a**), two modes (**b**), and three modes (**c**), respectively. (*Bottom panels*) Comparisons between the pre-defined GF-PDFs and the GF-PDFs inverted using Twomey's method with the optimized value of GF bins. The shaded area represents GF-PDF solution spaces within one standard deviation.

To quantify the accuracy of the inverted GF-PDFs, we fitted the inverted GF-PDFs to recover the mode parameters as shown in Table 1. The pre-set mode parameters of the pre-defined GF-PDFs are shown in Table 1. The results show that both the mode geometric means and the multimodal number fractions can be recovered accurately with minor uncertainties.

Table 2. Recovered mode parameters of pre-defined GF-PDFs from inverted GF-PDFs.

Predefined GF-PDF	Mode 1			Mode 2			Mode 3		
	f	G	σ	f	G	σ	f	G	σ
1	1.00 ± 0	1.39 ± 0.03	1.09 ± 0.01		NA			NA	
2	0.46 ± 0.10	1.10 ± 0.02	1.02 ± 0.01	0.54 ± 0.10	1.30 ± 0.02	1.03 ± 0.01		NA	
3	0.37 ± 0.09	1.05 ± 0.03	1.05 ± 0.02	0.34 ± 0.13	1.40 ± 0.03	1.03 ± 0.02	0.28 ± 0.12	1.69 ± 0.08	1.06 ± 0.03

4 Conclusion

In this study, we develop and evaluate nonparametric regularized methods for inverting GF-PDF from HFIMS measurements. The integrated response of HFIMS, which is a convolution of the aerosol hygroscopic GF-PDF, the transfer function of the DMA, and the transfer function of the WFIMS, is first cast into a matrix form. With the matrix form, nonparametric regularized methods can be applied straightforwardly to invert the GF-PDF. Synthetic HFIMS measurements are generated using Monte-Carlo simulations for representative aerosol GF-PDFs, and the synthetic data are used to investigate the dependence of inverted GF-PDF on the number of GF bins (i.e., GF resolutions) and the performances of different inversion methods. We show an optimal GF bin number of 20 for all nonparametric methods and representative

GF-PDFs. The performances of unregularized least-squares, Twomey's algorithm, Tikhonov regularizations, and commonly used parametric inversion methods (i.e., ML and PL least-squares fitting) are compared. Nonparametric methods based on the matrix form have substantial advantages in the inversion of GF-PDF over the parametric fitting methods as (1) no prior assumption of GF-PDF distributions is required; (2) the matrix-based form facilitates the application of different regularizations (e.g., Tikhonov regularization and Twomey's iterative regularization), which reduce the error in inverted GF-PDF by eliminating noise amplification; (3) they are much more computationally efficient once the matrix is generated. On average, The GF-PDF inverted using Twomey's method has the smallest error compared to solutions using the other inversion methods regardless of the shapes of the pre-defined GF-PDFs, and it accurately reproduces the true GF-PDF, including the mode parameters and other key statistics.

Data availability. Datasets and code packages related to this paper will be provided by the corresponding author (Jian Wang, jian@wustl.edu) upon request.

Author contributions. JZ and JW designed the study. JZ developed the code. JZ and JW prepared the manuscript with contributions from all co-authors.

Competing interests. The authors declare that they have no conflict of interest.

Acknowledgements. We acknowledge the funding support from the U. S. Department of Energy's Small Business Innovation Research (SBIR) program under contract DE-SC0013103 and Small Business Technology Transfer (STTR) program under contract DESC0006312.

References

Collins, D. R., Flagan, R. C., and Seinfeld, J. H.: Improved Inversion of Scanning DMA Data, Aerosol Science and Technology, 36, 1-9, 10.1080/027868202753339032, 2002.

Gysel, M., Crosier, J., Topping, D. O., Whitehead, J. D., Bower, K. N., Cubison, M. J., Williams, P. I., Flynn, M. J., McFiggans, G. B., and Coe, H.: Closure study between chemical composition and hygroscopic growth of aerosol particles during TORCH2, Atmos. Chem. Phys., 7, 6131-6144, 10.5194/acp-7-6131-2007, 2007.

Gysel, M., McFiggans, G. B., and Coe, H.: Inversion of tandem differential mobility analyser (TDMA) measurements, Journal of Aerosol Science, 40, 134-151, https://doi.org/10.1016/j.jaerosci.2008.07.013, 2009.

Hansen, P. C.: Analysis of Discrete Ill-Posed Problems by Means of the L-Curve, SIAM Review, 34, 561-580, 10.1137/1034115, 1992.

Hansen, P. C., and O'Leary, D. P.: The Use of the L-Curve in the Regularization of Discrete Ill-Posed Problems, SIAM Journal on Scientific Computing, 14, 1487-1503, 10.1137/0914086, 1993.

Hansen, P. C.: REGULARIZATION TOOLS: A Matlab package for analysis and solution of discrete ill-posed problems, Numerical Algorithms, 6, 1-35, 10.1007/BF02149761, 1994.

Kandlikar, M., and Ramachandran, G.: INVERSE METHODS FOR ANALYSING AEROSOL SPECTROMETER
335   MEASUREMENTS: A CRITICAL REVIEW, Journal of Aerosol Science, 30, 413-437, https://doi.org/10.1016/S0021-8502(98)00066-4, 1999.

Liu, B. Y. H., Pui, D. Y. H., Whitby, K. T., Kittelson, D. B., Kousaka, Y., and McKenzie, R. L.: The aerosol mobility chromatograph: A new detector for sulfuric acid aerosols, Atmospheric Environment (1967), 12, 99-104,
340   https://doi.org/10.1016/0004-6981(78)90192-0, 1978.

Markowski, G. R.: Improving Twomey's Algorithm for Inversion of Aerosol Measurement Data, Aerosol Science and Technology, 7, 127-141, 10.1080/02786828708959153, 1987.

345   Olfert, J. S., Kulkarni, P., and Wang, J.: Measuring aerosol size distributions with the fast integrated mobility spectrometer, Journal of Aerosol Science, 39, 940-956, https://doi.org/10.1016/j.jaerosci.2008.06.005, 2008.

Petters, M. D.: A Software Package to Simplify Tikhonov Regularization with Examples for Matrix-Based Inversion of SMPS and HTDMA Data, Atmos. Meas. Tech. Discuss., 2021, 1-27, 10.5194/amt-2021-51, 2021.
350
Pilinis, C., Pandis, S. N., and Seinfeld, J. H.: Sensitivity of direct climate forcing by atmospheric aerosols to aerosol size and composition, Journal of Geophysical Research: Atmospheres, 100, 18739-18754, https://doi.org/10.1029/95JD02119, 1995.

Pinterich, T., Spielman, S. R., Hering, S., and Wang, J.: A water-based fast integrated mobility spectrometer (WFIMS) with
355   enhanced dynamic size range, Aerosol Science and Technology, 51, 1212-1222, 10.1080/02786826.2017.1338664, 2017a.

Pinterich, T., Spielman, S. R., Wang, Y., Hering, S. V., and Wang, J.: A humidity-controlled fast integrated mobility spectrometer (HFIMS) for rapid measurements of particle hygroscopic growth, Atmos. Meas. Tech., 10, 4915-4925, 10.5194/amt-10-4915-2017, 2017b.
360
Rader, D. J., and McMurry, P. H.: Application of the tandem differential mobility analyzer to studies of droplet growth or evaporation, Journal of Aerosol Science, 17, 771-787, https://doi.org/10.1016/0021-8502(86)90031-5, 1986.

Rawat, V. K., Buckley, D. T., Kimoto, S., Lee, M.-H., Fukushima, N., and Hogan, C. J.: Two dimensional size–mass
365   distribution function inversion from differential mobility analyzer–aerosol particle mass analyzer (DMA–APM) measurements, Journal of Aerosol Science, 92, 70-82, https://doi.org/10.1016/j.jaerosci.2015.11.001, 2016.

Sipkens, T. A., Olfert, J. S., and Rogak, S. N.: Inversion methods to determine two-dimensional aerosol mass-mobility distributions: A critical comparison of established methods, Journal of Aerosol Science, 140, 105484,
370   https://doi.org/10.1016/j.jaerosci.2019.105484, 2020.

Stolzenburg, M., and McMurry, P.: TDMAFIT user's manual, University of Minnesota, Department of Mechanical Engineering, Particle Technology Laboratory, Minneapolis, 1-61, 1988.

375   Stolzenburg, M. R., and McMurry, P. H.: Equations Governing Single and Tandem DMA Configurations and a New Lognormal Approximation to the Transfer Function, Aerosol Science and Technology, 42, 421-432, 10.1080/02786820802157823, 2008.

Swietlicki, E., Hansson, H.-C., Hämeri, K., Svenningsson, B., Massling, A., McFiggans, G., McMurry, P. H., Petäjä, T.,
380   Tunved, P., and Gysel, M.: Hygroscopic properties of submicrometer atmospheric aerosol particles measured with H-TDMA
instruments in various environments—a review, Tellus B: Chemical and Physical Meteorology, 60, 432-469, 2008.

Talukdar, S. S., and Swihart, M. T.: An Improved Data Inversion Program for Obtaining Aerosol Size Distributions from
Scanning Differential Mobility Analyzer Data, Aerosol Science and Technology, 37, 145-161, 10.1080/02786820300952,
385   2003.

Tang, I., and Munkelwitz, H.: Aerosol phase transformation and growth in the atmosphere, Journal of Applied Meteorology,
33, 791-796, 1994.

390   Twomey, S.: Comparison of constrained linear inversion and an iterative nonlinear algorithm applied to the indirect
estimation of particle size distributions, Journal of Computational Physics, 18, 188-200, https://doi.org/10.1016/0021-
9991(75)90028-5, 1975.

Wang, Y., Pinterich, T., and Wang, J.: Rapid measurement of sub-micrometer aerosol size distribution using a fast integrated
395   mobility spectrometer, Journal of Aerosol Science, 121, 12-20, https://doi.org/10.1016/j.jaerosci.2018.03.006, 2018.

Wang, Y., Zheng, G., Spielman, S. R., Pinterich, T., Hering, S. V., and Wang, J.: Retrieval of high time resolution growth
factor probability density function from a humidity-controlled fast integrated mobility spectrometer, Aerosol Science and
Technology, 53, 1092-1106, 2019.
400
Zhang, J., Spielman, S., Wang, Y., Zheng, G., Gong, X., Hering, S., and Wang, J.: Rapid measurement of RH-dependent
aerosol hygroscopic growth using a humidity-controlled fast integrated mobility spectrometer (HFIMS), Atmos. Meas.
Tech., 14, 5625-5635, 10.5194/amt-14-5625-2021, 2021.

405   Zheng, G., Kuang, C., Uin, J., Watson, T., and Wang, J.: Large contribution of organics to condensational growth and
formation of cloud condensation nuclei (CCN) in the remote marine boundary layer, Atmospheric Chemistry and Physics,
20, 12515-12525, 2020.